Chen Chen, Yi Han, Yan Chen, and K.J. Ray Liu

# Indoor Global Positioning System with Centimeter Accuracy Using Wi-Fi

The global positioning system (GPS) is a space-based navigation system that can provide location and time information whenever there is an unobstructed line of sight (LOS) to four or more GPS satellites [1]. Such a system provides critical capabilities to military, civil, and commercial applications around the world. On the other hand, considering the fact that people today spend more than 80% of their time in indoor environments, accurate indoor localization is highly desirable and has a great potential impact on many applications. Unfortunately, the use of GPS satellites to enable indoor localization is a nonstarter due to a variety of reasons including poor signal strength, multipath effect, and limited on-device computation and communication power [2]. Therefore, over the past two decades, the research community has

been urgently seeking new technologies that can enable high-accuracy indoor localization. However, the results are still mostly unsatisfactory. Microsoft hosted Indoor Localization Competitions in recent years and concluded that "the indoor location problem is not solved" [3].

Many indoor positioning systems (IPSs) have been developed by leveraging radio wave, magnetic field, acoustic signal, or other sensory information collected by mobile devices [4]. Most of these systems are based on the ranging technique. Ranging is a process to determine the distance from one location to another by utilizing the collected information such as the received signal strength indicator (RSSI) and/or time of arrival (TOA). Typically, these systems require multiple anchors at known locations and dedicated devices to collect fine-grained information for accurate ranging.

However, when there exist obstacles between the localized device and the anchors, the localization performance degrades significantly. In other words, the performance of ranging-based systems cannot maintain under non-line-of-sight (NLOS) scenarios, which is very common for an indoor environment. Such degradation is due to that the physical ranging rules that translate the collected information into the distances are impaired by the blockage and multipath components naturally existing indoor. Developing a general physical ranging rule that suits NLOS conditions is practically difficult, if not impossible, due to the complicated indoor environment, which motivates the development of the fingerprint-based IPSs. A summary of the existing state-of-the-art capabilities from the Microsoft-hosted Indoor Localization Competitions is given in Figure 1, in

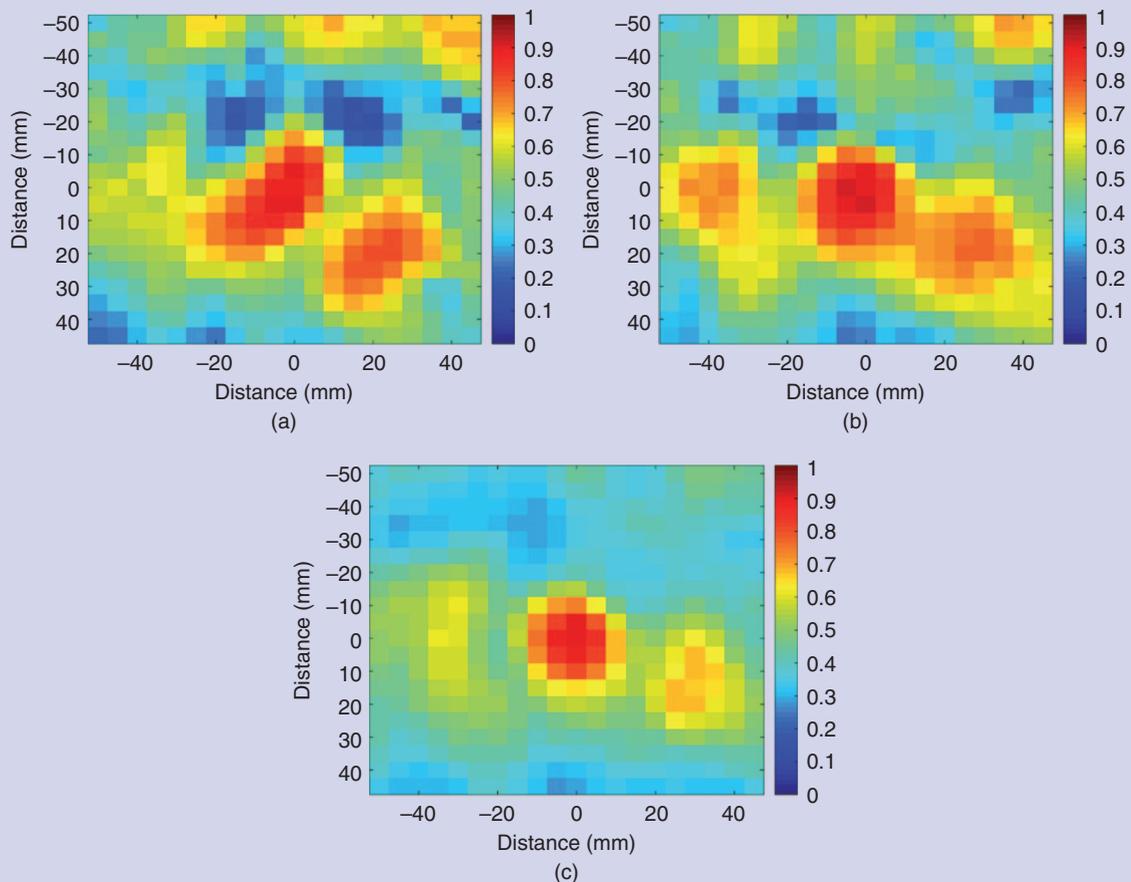| Technology | Existing Hardware? | Minimum Anchors | Low Cost? | Res. (m) LOS | Res. (m) NLOS | Commercial Examples |
|---|---|---|---|---|---|---|
| RSSI | ✓ | 3 | — | 1–3 | 5–10 | Active RFID, iBeacon, SPIRIT Navigation, Modulated LEDs |
| TOA TDOA | ✗ | 3 | ✗ | 0.2–0.4 | 1–5 | UWB, Decawave, Time Domain, Zebra, Nanotron |
| AOA | ✓ | 2 | — | 0.4 | 1–5 | None |
| Time Reversal | ✓ | 1 | ✓ | 0.02 | 0.02 | Origin Wireless |

**FIGURE 1.** State-of-the-art IPSs.

**FIGURE 2.** Ambiguity among nearby locations under (a) 40-MHz bandwidth, (b) 120-MHz bandwidth, and (c) 360-MHz bandwidth.

which one can see that under the LOS condition, with more than one anchor, submeter accuracy can be achieved. However, under the NLOS condition, only the meter range can be obtained by most methods, except the recently proposed time-reversal approach that can obtain 1–2 cm accuracy for both LOS and NLOS conditions [5].

In an indoor environment, there naturally exists some location-specific information, known as the fingerprints. Examples include the magnetic field, RSSI, and the channel state information (CSI). All of these fingerprints can be exploited for indoor localization. Specifically, in the fingerprint-based IPS, the location-specific fingerprints are collected and stored in a database in the mapping phase. Then, in the localization phase, the location of the device is determined by comparing the device fingerprint with those in the database.

In [5], it was shown that the physical phenomenon of the time-reversal focusing effect can provide a high-resolution fingerprint for indoor localization. The authors used a dedicated device to obtain the channel impulse response under the 5 GHz industrial, scientific, and medical radio (ISM) band with a bandwidth of 125 MHz as the fingerprint and utilized the time-reversal resonating strength (TRRS) as the similarity measure, which gives an accuracy of 1–2 cm.

The question now is: Can one use the ubiquitous Wi-Fi devices to achieve the same? The answer is yes as evidenced by the recent works in [6]–[8]. The work in [6] and [7] leveraged frequency hopping, while the work in [8] used multiantenna spatial diversity to increase the effective bandwidth. As a result, the localization resolution can be significantly improved to 1–2 cm.

This article will show the basic principles of how one can achieve indoor localization resolution down to the centimeter accuracy level using standard Wi-Fi devices. A unified view by combining both the frequency and spatial diversities is also presented.

## How does bandwidth affect the localization performance?

The main reason that most of the fingerprint-based methods utilizing CSI in Wi-Fi systems cannot achieve centimeter localization accuracy is due to the bandwidth limitation. More specifically, the maximum bandwidth in mainstream Wi-Fi devices is only either 20 or 40 MHz, which introduces severe ambiguity into the fingerprints of different locations and thus leads to the poor accuracy for indoor localization.

To clearly illustrate the impact of bandwidth on localization performance, we have conducted experiments to collect CSIs under different bandwidths in a typical indoor environment. Two channel sounders are placed in an NLOS setting, where one of them is placed on a customized experiment structure with 5-mm resolution.

To characterize the similarity between CSIs collected at the same or different locations, the TRRS is calculated, given by

$$\gamma[\mathbf{H}, \mathbf{H}'] = \left(\frac{\eta}{\sqrt{\Lambda}\sqrt{\Lambda'}}\right)^2, \qquad (1)$$

with

$$\eta = \max_{\phi}\left|\sum_{k=1}^{K} H_k H_k'^* e^{-jk\phi}\right|,$$

$$\Lambda = \sum_{k=1}^{K} |H_k|^2, \Lambda' = \sum_{k=1}^{K} |H_k'|^2, \quad (2)$$

where $\mathbf{H}$ and $\mathbf{H}'$ represent two fingerprints, $K$ is the total number of usable subcarriers, $H_k$ and $H_k'$ are the CSIs on subcarrier $k$, $\eta$ is the modified cross-correlation between $\mathbf{H}$ and $\mathbf{H}'$ with synchronization error compensated, and $\Lambda, \Lambda'$ are the channel energies of $\mathbf{H}$ and $\mathbf{H}'$, respectively. Realizing that the Wi-Fi receiver may not be fully synchronous with the Wi-Fi transmitter due to mismatches in their radio-frequency front-end components [9], an additional phase rotation of $e^{-jk\phi}$ is employed to counteract the phase distortions incurred by the synchronization errors in the calculation of $\eta$, where $\phi$ can be estimated and compensated using Algorithm 1 shown later in the section "Calculating Time-Reversal Resonating Strength by Diversity Exploitation." Equation (1) implies that TRRS ranges from 0 to 1. More specifically, a larger TRRS indicates a higher similarity between two fingerprints and thus the two associated locations.

The corresponding TRRS between the target location and nearby locations are illustrated in Figure 2 under different bandwidth settings. It is shown in Figure 2(a) that with 40 MHz bandwidth, a large region of nearby locations is ambiguous with the target location in terms of the TRRS. Enlarging the bandwidth shrinks the area of ambiguous regions. As

demonstrated in Figure 2(c), when the bandwidth increases to 360-MHz, the ambiguous region is reduced to a ball of 1 cm radius, which implies centimeter accuracy in localization.

The experiment results motivate us to formulate a large effective bandwidth by exploiting diversities on Wi-Fi devices to facilitate centimeter accuracy indoor localization.

## Increasing effective bandwidth via diversity exploitation

Two different diversities exist in the current Wi-Fi system, i.e., frequency diversity and spatial diversity. According to IEEE 802.11n, 35 Wi-Fi channels are dedicated to Wi-Fi transmission in 2.4- and 5-GHz-frequency bands with a maximum bandwidth of 40 MHz. The multitude of Wi-Fi channels leads to frequency diversity in that they provide opportunities for Wi-Fi devices to perform frequency hopping when experiencing deep fading or severe interference. On the other hand, spatial diversity can be exploited on multiple-input, multiple-out (MIMO) Wi-Fi devices, which is a mature technique that greatly boosts the spectral efficiency. MIMO has not only become an essential component of IEEE 802.11n/ac but also been ubiquitously deployed on numerous commercial Wi-Fi devices. For Wi-Fi systems, both types of diversity can be harvested to provide fingerprints with much finer granularity and thus lead to less ambiguity in comparison with the fingerprint measured with a bandwidth of only 40 MHz.

Figure 3 shows the general principle of creating a large effective bandwidth by exploiting the frequency and spatial diversities either independently or jointly. Since Wi-Fi devices can work on multiple Wi-Fi channels, one can exploit the frequency diversity by performing frequency hopping to obtain CSIs on different Wi-Fi channels. As demonstrated in Figure 3(a), CSIs on four different Wi-Fi channels are concatenated together to formulate a fingerprint of a large effective bandwidth. Despite the fact that the frequency diversity can be exploited on a single-antenna Wi-Fi device, it is

time-consuming to perform frequency hopping. For time efficiency, spatial diversity can be exploited on multiantenna Wi-Fi devices. For a Wi-Fi receiver with four antennas, e.g., in Figure 3(b), CSIs on the four receiving antennas can be combined together to formulate the fingerprint with a large effective bandwidth. Figure 3(c) shows an example of utilizing both the frequency and spatial diversities, where CSIs on two Wi-Fi channels and from two receiving antennas are combined into the fingerprint.

For a Wi-Fi system, the spatial diversity is determined by the number of antenna links, while the frequency diversity is dependent on the number of available Wi-Fi channels. Denote the maximum spatial diversity by $S$, the maximum frequency diversity by $F$, and the bandwidth for each Wi-Fi channel by $W$, the effective bandwidth is calculated as $S \times F \times W$.

## Achieving centimeter accuracy via TRRS

As discussed in the section "Increasing Effective Bandwidth via Diversity Exploitation," a fine-grained fingerprint associated with a large effective bandwidth can be generated through diversity exploitation on Wi-Fi devices. In this section, we first introduce the calculation of TRRS when both of the frequency and spatial diversities are available. Then, we present the algorithm for indoor localization.

### Calculating TRRS by diversity exploitation

As discussed in the sections "How Does Bandwidth Affect the Localization Performance?" and "Increasing Effective Bandwidth via Diversity Exploitation," to achieve centimeter localization accuracy, a large effective bandwidth beyond 40 MHz is required, which can be obtained by diversity exploitation. For Wi-Fi devices with a spatial diversity of $S$ and a frequency diversity of $F$, the CSI measurements can be written as $\overline{\mathbf{H}} = \{\mathbf{H}_{s,f}\}_{s=1,2,...,S}^{f=1,2,...,F}$, where $H_{s,f}$ stands for the CSI measured with the $s$th antenna link on the $f$th Wi-Fi channel, denoted as the virtual link $(s, f)$.
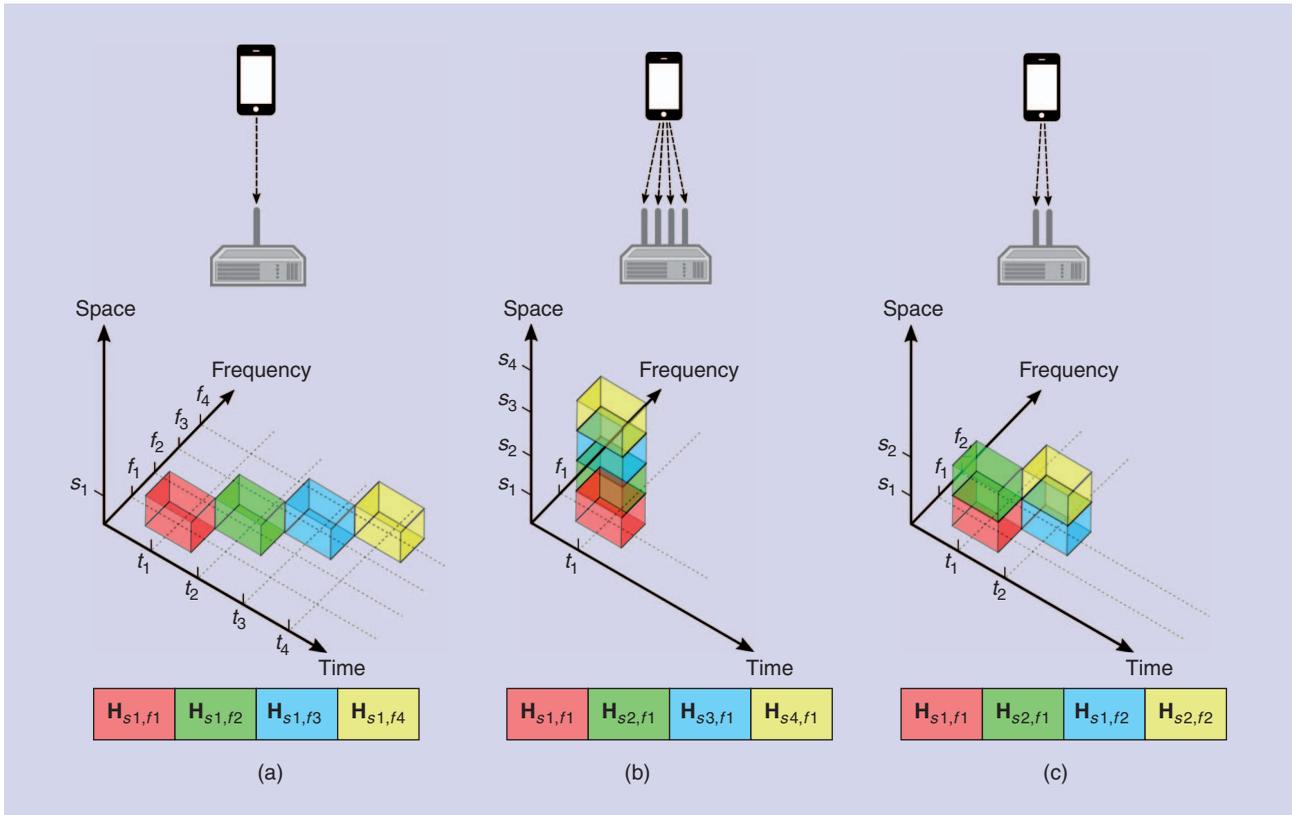
**FIGURE 3.** Leveraging frequency and spatial diversities in Wi-Fi to achieve large effective bandwidth: (a) using only the frequency diversity, (b) using only the spatial diversity, and (c) using both of the frequency and spatial diversities.

$\overline{\mathbf{H}} = \{\mathbf{H}_{s,f}\}_{s=1,2,\dots,S}^{f=1,2,\dots,F}$ can provide fine-grained fingerprint with an effective bandwidth of $S \times F \times W$. Consequently, TRRS in (1) can be extended to the fine-grained fingerprint $\overline{\mathbf{H}}$ and $\overline{\mathbf{H}}$, with $\eta$ and $\Lambda, \Lambda'$ modified as

$$\eta = \sum_{s=1}^{S} \sum_{f=1}^{F} \eta_{s,f},$$

$$\Lambda = \sum_{s=1}^{S} \sum_{f=1}^{F} \Lambda_{s,f}, \quad \Lambda' = \sum_{s=1}^{S} \sum_{f=1}^{F} \Lambda'_{s,f}, \quad (3)$$

where

$$\eta_{s,f} = \max_{\phi} \left| \sum_{k=1}^{K} H_{s,f,k} H'^{*}_{s,f,k} e^{-jk\phi} \right| \quad (4)$$

represents the modified cross-correlation on the virtual link $(s,f)$, and $\Lambda_{s,f} = \sum_{k=1}^{K} |H_{s,f,k}|^2$, $\Lambda'_{s,f} = \sum_{k=1}^{K} |H'_{s,f,k}|^2$ are the channel energies of $\mathbf{H}_{s,f}$ and $\mathbf{H}'_{s,f}$ on the virtual link $(s,f)$, respectively.

Algorithm 1 elaborates on the calculation of $\gamma[\overline{\mathbf{H}}, \overline{\mathbf{H}}']$. As shown in Algorithm 1, steps 4–9 are used to calculate

the channel energies on the virtual link $(s,f)$, while steps 10–14 are targeted to compute the modified cross-correlation of two CSIs on the virtual link $(s,f)$. The channel energies and modified cross-correlation on each virtual link are accumulated as shown in step 9 and step 15, respectively. Finally, the TRRS is obtained by step 18. The computation of $\eta_{s,f}$ is approximated by $\bar{\eta}_{s,f} = \max_n \left| \sum_{k=1}^{K} H_{s,f,k} H'^{*}_{s,f,k} e^{-j\frac{2\pi n(k-1)}{N}} \right|$ that takes the same format of a discrete Fourier transform of size $N$ and thus can be computed efficiently by fast Fourier transform. Using a large $N$ in the computations leads to a more accurate approximation of $\eta_{s,f}$.

## Localization using TRRS

There are two phases in the proposed IPS: a mapping phase and a localization

phase. During the mapping phase, the CSIs are collected from $L$ locations-of-interest using Wi-Fi devices with $S$ antenna links and across $F$ Wi-Fi channels, denoted by $\{\overline{\mathbf{H}}_\ell\}_{\ell=1,2,\dots,L}$. In the localization phase, $\overline{\mathbf{H}}'$ is obtained at a testing location, which may either be one of the $L$ locations-of-interest or an unmapped location in the mapping phase. Then, the pairwise TRRS $\gamma[\overline{\mathbf{H}}_\ell, \overline{\mathbf{H}}']$, is calculated for all locations-of-interest. Finally, the location is determined based on $\gamma[\overline{\mathbf{H}}_\ell, \overline{\mathbf{H}}]$, i.e, (5), shown in the box at the bottom of the page, where $\Gamma$ is a threshold introduced to balance off the true positive rate and false positive rate in location determination. When $\gamma[\overline{\mathbf{H}}_\ell, \overline{\mathbf{H}}']$ falls below $\Gamma$, the IPS cannot obtain a credible location estimation and returns 0 to imply an unmapped location.

$$\hat{\ell} = \begin{cases} \underset{\ell=1,2,\dots,L}{\arg\max} \gamma[\overline{\mathbf{H}}_\ell, \overline{\mathbf{H}}'], & \text{If } \underset{\ell=1,2,\dots,L}{\max} \gamma[\overline{\mathbf{H}}_\ell, \overline{\mathbf{H}}'] \geq \Gamma \\ 0, & \text{Otherwise} \end{cases} \quad (5)$$
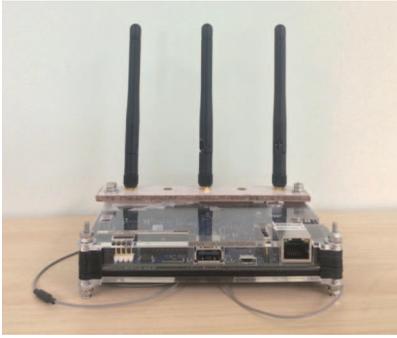
**FIGURE 4.** The Wi-Fi device used in the proposed IPS.

## Experiment results

Extensive experiments are conducted to validate the theoretical analysis and evaluate the performance of the proposed IPS. The proposed system contains two Wi-Fi devices, each equipped with three omnidirectional antennas. One Wi-Fi device, called Origin, estimates CSI from the other Wi-Fi device, named the Bot. With the proposed algorithm in the section "Achieving Centimeter Accuracy Via TRRS," the Origin estimates the location of the Bot. Figure 4 shows one Wi-Fi device used in the proposed IPS.

The experiments are conducted in a typical office of a multistory building. The indoor space is filled with a large number of reflectors, e.g., chairs, desks, shelves, sofas, walls, and ceilings. The CSIs of 50 candidate locations are measured, with 20 measurements for each location.

To evaluate the performance, the CSIs at each location are partitioned into a training set and a testing set, with ten CSIs for each. The TRRS matrix is calculated using the CSIs collected at the 50 candidate locations. Each element of the matrix represents the TRRS between the CSIs at the training location and the testing location. In other words, the diagonal elements of the matrix indicate the similarity between CSIs at the same location, while the off-diagonal elements stand for the similarity between CSIs of different locations.

Figure 5 illustrates the TRRS vmatrices under effective bandwidths of 10, 40, 120, and 360 MHz. First of all, it is easily seen from Figure 4 that the diagonal elements of the matrices are close to one, signifying high similarities among CSIs of the same locations. Regarding the off-diagonal elements, they become smaller with an increasing effective bandwidth. When the effective bandwidth is small, e.g., 10 MHz, some off-diagonal elements are even larger than the diagonal elements, giving rise to localization errors. In other words, it is very likely to localize the Bot to incorrect positions when the effective bandwidth is small. When the effective bandwidth is increased, the gap between diagonal and off-diagonal elements enlarges, which provides a clear watershed between the correct and incorrect locations and leads to an enhanced system performance in return.

To provide a statistical point of view, Figure 6 shows the cumulative density functions of the diagonal and off-diagonal elements in TRRS matrices under a variety of effective bandwidths. As we can see, the gap between the diagonal and off-diagonal elements increases with the effective bandwidth, indicating a better distinction between different locations. Whenever there is a gap between the diagonal and off-diagonal elements, a perfect localization can be achieved with an appropriate threshold, i.e., 100% true positive rate and 0% false positive rate.

In a practical indoor environment, there usually exists environment dynamics that might degrade the localization performance. To evaluate the proposed IPS in a dynamic indoor environment, the testing CSIs are recollected in the presence of human activities and large object movement. In particular, to emulate dynamics from human activities, one participant was asked to walk continuously in the vicinity of the Bot. Then, the participant was asked to open and close a door that blocks the direct link between the Origin and Bot so as

---

**Algorithm 1. Calculating TRRS by exploiting diversities.**

**Input:** $\overline{\mathbf{H}} = \{\mathbf{H}_{s,f}\}_{s=1,2,\ldots,S}^{f=1,2,\ldots,F}$, $\overline{\mathbf{H}}' = \{\mathbf{H}'_{s,f}\}_{s=1,2,\ldots,S}^{f=1,2,\ldots,F}$

**Output:** $\gamma[\overline{\mathbf{H}}, \overline{\mathbf{H}}']$

1: $\Lambda = 0, \Lambda' = 0, \eta = 0$

2: **for** $s = 1, 2, \ldots, S$ **do**

3:     **for** $f = 1, 2, \ldots, F$ **do**

4:         $\Lambda_{s,f} = 0, \Lambda'_{s,f} = 0$

5:         **for** $k = 1, 2, \ldots, K$ **do**

6:             $\Lambda_{s,f} \leftarrow \Lambda_{s,f} + |H_{s,f,k}|^2$

7:             $\Lambda'_{s,f} \leftarrow \Lambda'_{s,f} + |H'_{s,f,k}|^2$

8:         **end for**    } Calculating channel energies on virtual link $(s, f)$

9:         $\Lambda \leftarrow \Lambda + \Lambda_{s,f}, \ \Lambda' \leftarrow \Lambda' + \Lambda'_{s,f}$

10:         **for** $n = 1, 2, \ldots, N$ **do**

11:             $z[n] \leftarrow \sum_{k=1}^{N} H_{s,f,k} H'^{*}_{s,f,k} e^{-j\frac{2\pi n(k-1)}{N}}$

12:         **end for**    } Calculating modified cross-correlation on virtual link $(s, f)$

13:         $n^{\star} = \underset{n=1,2,\ldots,N}{\arg\max} |z[n]|$

14:         $\bar{\eta}_{s,f} = z[n^{\star}]$

15:         $\eta \leftarrow \eta + \bar{\eta}_{s,f}$

16:     **end for**

17: **end for**

18: $\gamma[\overline{\mathbf{H}}, \overline{\mathbf{H}}'] \leftarrow \left(\frac{\eta}{\sqrt{\Lambda}\sqrt{\Lambda}}\right)^2$
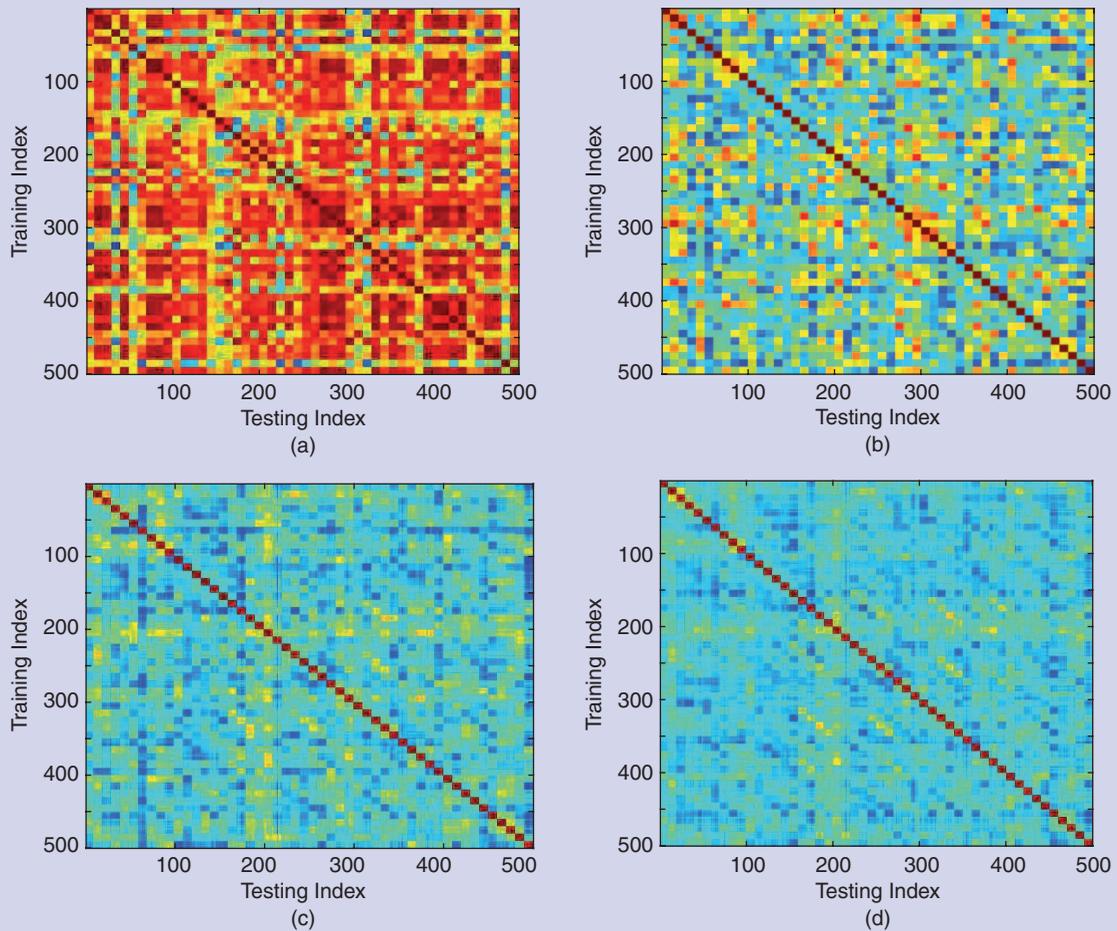
---

**FIGURE 5.** The TRRS matrix under an effective bandwidth of (a) 10 MHz, (b) 40 MHz, (c) 120 MHz, and (d) 360 MHz.
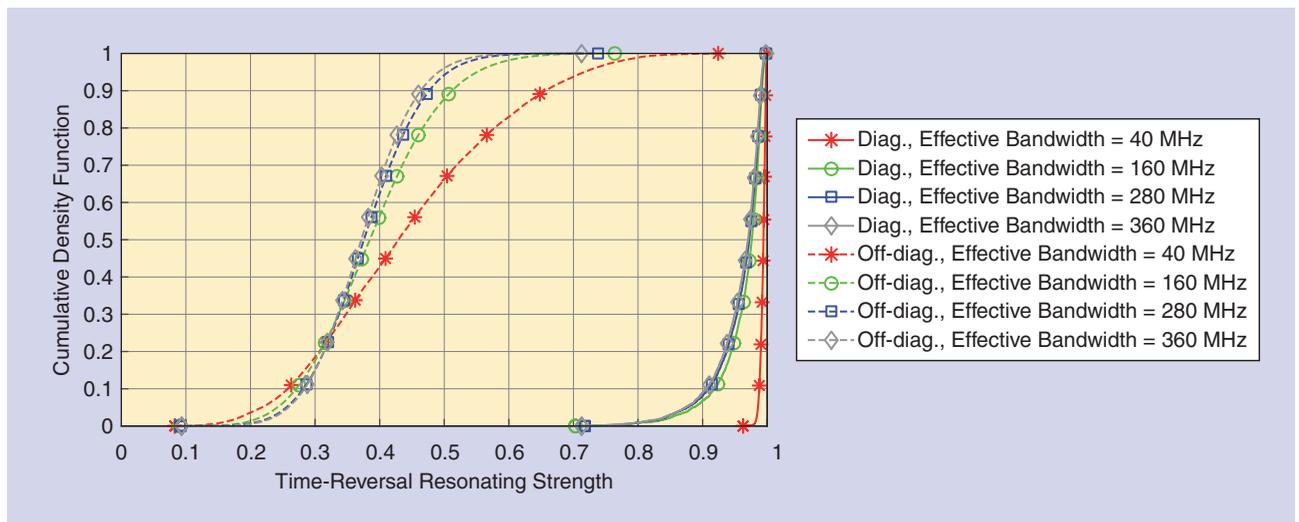


**FIGURE 6.** Cumulative density functions of the TRRS of the diagonal and off-diagonal elements.

to emulate the dynamics from large object movement.

Figure 7(a) demonstrates the receiver operating characteristic curve with human activities. For a fixed false positive rate 0.15%, the true positive rate increases from 94.17% with 40-MHz effective bandwidth to 99.11% with 120-MHz effective bandwidth. Further enlarging the effective bandwidth to 240 MHz and 360 MHz boosts the true positive rate to 99.61% and 99.89%,
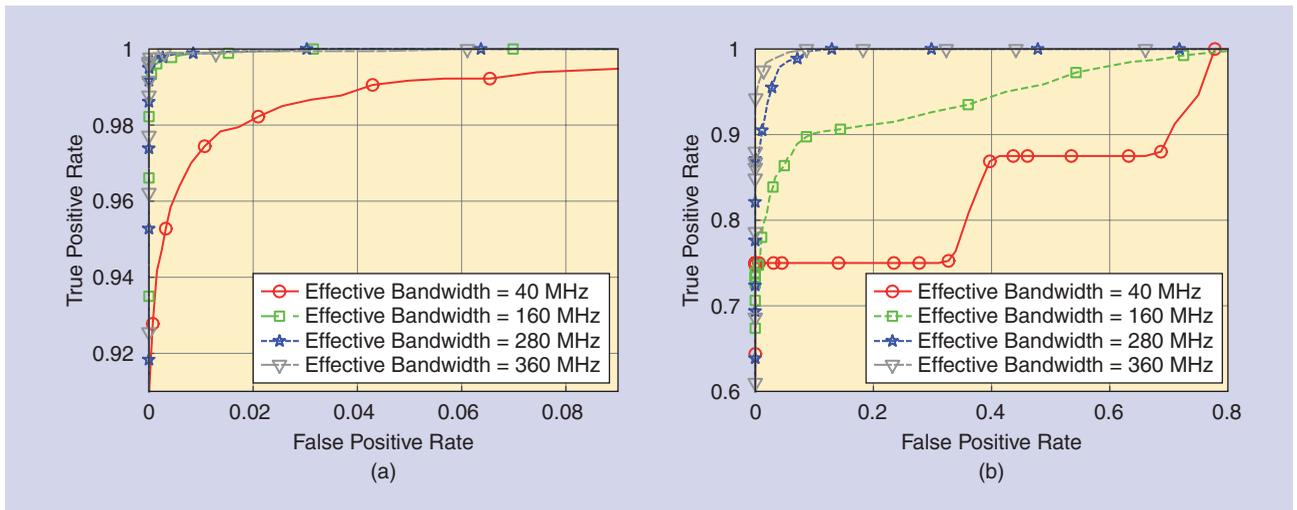
**FIGURE 7.** The receiver operating characteristic curve in the presence of environment dynamics: (a) dynamics from human movement and (b) dynamics from door opening and closing.

respectively. On the other hand, Figure 7(b) depicts the receiver operating characteristic curve with large object movement. For a fixed false positive rate 0.15%, the true positive rate increases from 75% with 40 MHz effective bandwidth to 76.38, 87.12, and 95% with 120, 240, and 360 MHz effective bandwidths, respectively. This can be justified by that, with a large effective bandwidth, the environment dynamics only affect very limited information in the fingerprint while leaving the majority intact. In other words, a large effective bandwidth enhances the robustness of the proposed IPS against environment dynamics.

During the experiments, we observe multiple Wi-Fi access points coexisting with the proposed IPS. However, their impact on the proposed IPS is minimal. Due to the carrier sense multiple access with collision avoidance (CSMA/CA) mechanism, these Wi-Fi access points would not transmit signals whenever they sense that the IPS is operating to obtain CSIs, which guarantees that the captured CSIs are free from interference.

## Conclusions

In this column, we present a time-reversal method for indoor localization that achieves centimeter accuracy with a single pair of off-the-shelf Wi-Fi devices. The high accuracy for localization is maintained under strong NLOS scenarios. With the exploitation of the inherent frequency and spatial diversities in Wi-Fi systems, it is capable of creating a large effective bandwidth to enable centimeter accuracy. Extensive experiment results in a typical office environment show that the centimeter accuracy as well as robustness against dynamics can be simultaneously achieved with a large effective bandwidth. The global GPS can achieve 3–15 m of accuracy by mapping the world into latitude and longitude coordinates. The presented "indoor GPS" can achieve 1–2 cm accuracy when an indoor environment is fingerprinted and mapped.

## Authors

*Chen Chen* (cc8834@umd.edu) is a graduate student of the Department of Electrical and Computer Engineering, University of Maryland, College Park. He is also affiliated with Origin Wireless.

*Yi Han* (yi.han@originwireless.net) received his Ph.D. degree from the Department of Electrical and Computer Engineering, University of Maryland, College Park. Currently, he is the wireless architect of Origin Wireless.

*Yan Chen* (eecyan@uestc.edu.cn) is a professor with the School of Electronic Engineering, University of Electronic Science and Technology of China. He was a principal technologist of Origin Wireless.

*K.J. Ray Liu* (kjrliu@umd.edu) is the founder of Origin Wireless. He is also the Christine Kim Eminent Professor of Information Technology at the University of Maryland, College Park.

## References

[1] J. G. McNeff, "The global positioning system," *IEEE Trans. Microwave Theory Tech.*, vol. 50, pp. 645–652, Mar. 2002.

[2] S. Nirjon, J. Liu, G. DeJean, B. Priyantha, Y. Jin, and T. Hart, "Coin-GPS: Indoor localization from direct GPS receiving," in *Proc. ACM 12th Annu. Int. Conf. Mobile Systems, Applications, and Services*, 2014, pp. 301–314.

[3] D. Lymberopoulos, J. Liu, X. Yang, R. R. Choudhury, S. Sen, and V. Handziski, "Microsoft Indoor Localization Competition: IPSN 2016," *GetMobile: Mobile Comp. and Comm.* [Online]. Available: http://doi.acm.org/10.1145/2721914.2721923

[4] K. Curran, E. Furey, T. Lunney, J. Santos, D. Woods, and A. McCaughey, "An evaluation of indoor location determination technologies," *J. Location Based Services*, vol. 5, no. 2, pp. 61–78, 2011.

[5] Z.-H. Wu, Y. Han, Y. Chen, and K. J. R. Liu, "A time-reversal paradigm for indoor positioning system," *IEEE Trans. Veh. Technol.*, vol. 64, no. 4, pp. 1331–1339, 2015.

[6] C. Chen, Y. Chen, H. Q. Lai, Y. Han, and K. J. R. Liu, "High accuracy indoor localization: A WiFi-based approach," in *Proc. IEEE Int. Conf. Acoustics, Speech and Signal Processing*, 2016, pp. 6245–6249.

[7] C. Chen, Y. Chen, Y. Han, H. Lai, and K. J. R. Liu, "Achieving centimeter accuracy indoor localization on Wi-Fi platforms: A frequency hopping approach," *IEEE Trans. Internet Things*, to be published.

[8] C. Chen, Y. Chen, Y. Han, H. Lai, F. Zhang, and K. J. R. Liu, "Achieving centimeter accuracy indoor localization on Wi-Fi platforms: A multi-antenna approach," *IEEE Trans. Internet Things*, to be published.

[9] M. Speth, S. Fechtel, G. Fock, and H. Meyr, "Optimum receiver design for wireless broad-band systems using OFDM—Part I," *IEEE Trans. Commun.*, vol. 47, pp. 1668–1677, Nov. 1999.

**SP**